Integrating Materials and Manufacturing Innovation (2018) 7:136–147
https://doi.org/10.1007/s40192-018-0115-x

TECHNICAL ARTICLE

An ICME Framework for Design of Stainless Steel for Sintering

Tesfaye T. Molla[1] · J. Z. Liu[1] · G. B. Schaffer[1]

Received: 22 June 2018 / Accepted: 9 July 2018 / Published online: 23 July 2018

Abstract

Recent progress in the development of integrated computational materials engineering (ICME) models offers new capabilities to deal with the challenge of designing multi-component alloys. In this study, a new type of computational method for efficient design of sintered stainless steel alloys, optimized for manufacturability (sintering) as well for performance, is presented. Development of the design method follows the materials systems approach that integrates processing, structure, and property relations during metal injection molding (MIM). It includes a multi-objective genetic algorithm (GA) to optimize alloy composition with the aim of improving the sintering as well as performance-related properties. To achieve this, the GA is coupled with computational thermodynamics and predictive analytical models. Thermodynamic simulations, based on the calculation of phase diagram CALPHAD method, are used to establish constraints through phase stability at equilibrium and calculate the diffusivity that determines the sintering behavior of the alloy. In addition, an advanced predictive model is used to determine solution strengthening. To demonstrate the capability of our method, a design exercise for austenitic stainless steel is presented. New alloys which are optimized for improved sinterability, yield strength, corrosion resistance, and cost are compared to 316L, a commercially available austenitic steel that is widely produced by MIM.

Keywords Integrated computational materials engineering (ICME) · Alloy design · Stainless steel · Metal injection molding · Sintering · Powder metallurgy

Introduction

The current design of alloys typically occurs through an evolutionary-like, random walk process, requiring many thousands of experiments to develop empirical correlations, which often have poor predictive capability for performance-related properties. Furthermore, design optimizations based on such correlations usually do not offer the necessary flexibility to incorporate multiple and sometimes competing objectives. The challenge becomes explosively large during the design of multi-component alloys coupled with materials processing parameters. For these reasons, traditional alloy design usually results in long development timelines, sometimes over decades, at excessive cost. It is therefore desirable to develop an efficient framework for the design of alloys that can handle multiple and possibly conflicting objectives and/or constraints.

In an age of increasing cost of experiments and decreasing cost of computation, a design approach making the maximum use of science-based mechanistic models and a small number of experiments significantly reduces the time and cost of alloy development [1]. Computational methods are particularly useful in the design of multi-component alloys, like stainless steels, which can contain more than eight alloying elements. Furthermore, computational designs can also allow the development of complex algorithms in a way not only to optimize the powder mix for performance-related properties but also to enhance manufacturability and consider other attributes such as cost.

Computational design of alloys involves algorithms and tools that have the potential to scan vast compositional space to determine the right combination of composition and process parameters. The ideal approach is through the development of physics-based models that deal with hierarchical structural problems. Hierarchal models representing the corresponding problems at different time and length scales then need to be integrated with each other to predict properties of the product [2]. Furthermore, these models need to be coupled

✉ Tesfaye T. Molla
tesfaye.molla@unimelb.edu.au

[1] Department of Mechanical Engineering, The University of Melbourne, Parkville Campus, Building 166, Melbourne, Victoria 3010, Australia

with search algorithms to explore the possible compositional space. However, these kinds of models are often very complex requiring not only huge and efficient computational infrastructure but also comprehensive databases and well-developed and systematically integrated algorithms that can run simultaneously at different time and length scales.

There are two approaches to simplifying computational design of alloys without the need for developing multi-scale or hierarchical models. The first involves integration of phase-based models and data mining using, for example, artificial neural network (ANN) or Gaussian processes, coupled with search algorithms. Multi-objective design of metallic alloys using computational thermodynamics-driven genetic algorithm (GA) and evaluation of material behaviors using Gaussian process are studied extensively by Tancret et al. [3–5], Jha et al. [6], Mahfouf et al. [7], and Manou et al. [8]. Manou et al. were able to demonstrate a computational design approach using a multi-criteria, multi-objective genetic algorithm coupled with ThermoCalc (TC), a computational thermodynamics and material database software, and Gaussian method [8]. An essential part of this study was the control of the precipitation of the γ' strengthening phase and the resultant high-temperature properties. However, artificially trained models often work well within the range of data they are trained in but their predictive capability drops quickly outside the data domain. This limits the usefulness of artificially trained models to explore unoccupied compositional space during the development of multi-component alloys.

The second approach is through the integration of phase-based models with physics-based mechanical property models. In this regard, Li et al. reported a computational design methodology for high work-to-necking Ni-ternary alloys by integrating the simulation of γ' precipitation using ThermoCalc with mechanical property models coupled to a genetic algorithm [9]. The reliability of this approach will depend on the predictive capability of the property models used in the computational design framework. Advanced mechanical property models that can offer the necessary flexibility during the development of integrated computational design methods for alloys are being developed, such as that by Walbruhl et al. [10] to predict solid solution strengthening in multi-component alloys. This approach facilitates the development of advanced physics-based mechanical property models that can be coupled to phase-based models to develop simplified methodologies for the computational design of alloys.

Here, a computational framework for the design of multi-component alloys is developed by integrating (1) computational thermodynamics to establish microstructural constraints and determine a kinetic parameter affecting the processing of alloys for powder metallurgy (PM) and (2) predictive models to evaluate performance properties as well as cost. These tools are coupled to a multi-objective genetic algorithm to search and optimize the sintering behavior and performance-related properties. For the purpose of demonstration, the design of an austenitic stainless steel alloy produced by PM through metal injection molding (MIM) is considered. This system is chosen because it is commercially important and can also be modeled with a reduced set of critical parameters. In addition, MIM has the further advantage of being a growing industry sector that uses a limited number of conventional wrought stainless steel alloys. During the design, candidate austenitic stainless steel alloys are optimized to maximize the sintering behavior (improved densification), yield strength, and pitting corrosion resistance while minimizing the cost. The design method involves a search algorithm based on a GA, coupled to the capabilities of TC for calculating phase equilibria and evaluating the effective self-diffusivities of alloys. In addition, predictive models for determining the change in solution hardening, pitting corrosion resistance, and cost are also considered. The sintering behavior as well as change in yield strength from the resulting optimal alloys are compared with 316L, a commonly used austenitic stainless steel, which is also fabricated by MIM. The design methodology is implemented using Matlab™ coupled with TC through the TC-Matlab interface.

Material Systems for Stainless Steel Produced by MIM

The present study follows the material systems approach suggested by Olsen [1] to integrate processing, structure, and property (PSP) relations for the design of an austenitic stainless steel produced by the MIM process. The material property objectives include yield strength, toughness, corrosion resistance, and cost. The set of property objectives are thus used as a foundation to build a first order representation of a full material system chart for MIM, see Fig. 1. This type of chart helps to explicitly represent the microstructural subsystems controlling the properties of interest and the substages of processing governing the evolution of each subsystem. In addition, the material system chart can be used to prioritize the PSP links and develop an inductive goal to achieve the necessary properties.

In this study, a design exercise is performed for an austenitic stainless steel alloy of minimal cost with improved yield strength and pitting corrosion resistance. The target microstructure is austenite with a fine grain size and minimal porosity (higher density). These structural requirements are primarily controlled through the design of the base powder mix (composition and particle size) and the sintering processes. This is apparent by the large number of lines linking those two processes (base powder preparation and sintering) to the structural goals as shown in Fig. 1. In addition, the design of the base powder composition can also affect the sintering behavior of the powder compact (green body of the alloy), through the

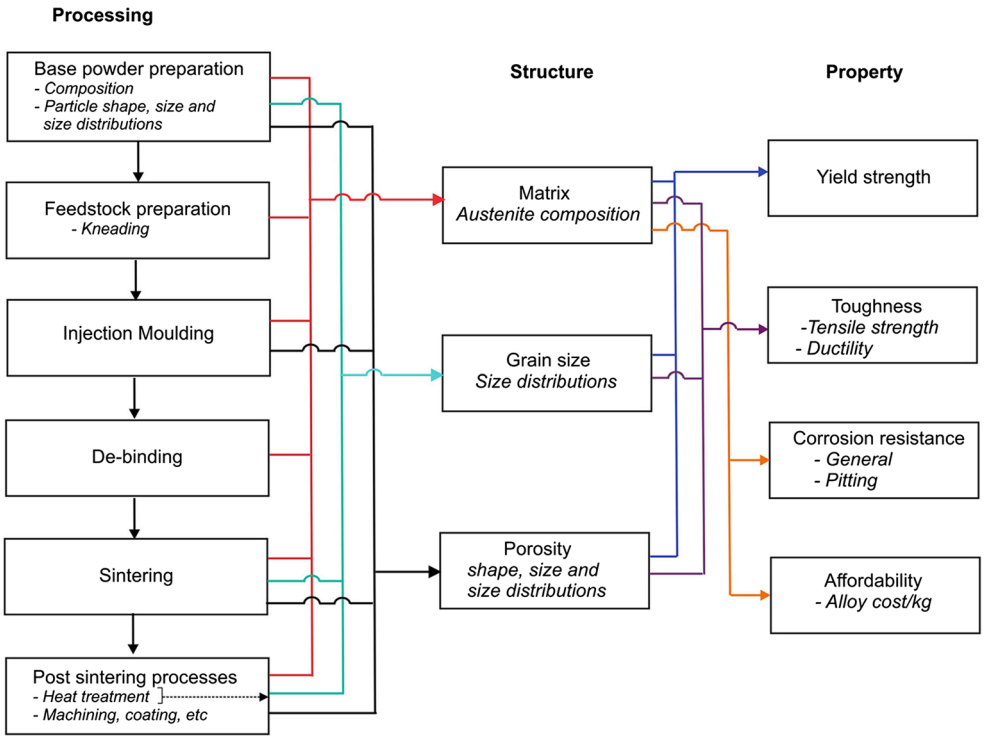

Fig. 1 Material system chart for an austenitic stainless steel alloy manufactured by MIM

vertical flowchart showing the evolution of process steps. Thus, the base powder preparation is the critical processing step in the design of alloy with the necessary properties.

To enable an efficient search algorithm, the following assumptions and requirements are made:

1. The powder compact is assumed to constitute a uniform dispersion of mono-sized particles. This is typical for a MIM feedstock and avoids the need to account for factors related with a powder having different particle sizes and shapes.
2. The composition should result in a single-phase austenitic structure at the sintering temperature. This removes the need to account for multi-phase structures and is typical of many conventional stainless steels.
3. Densification during solid-state sintering of a powder compact with a uniform dispersion of mono-sized particles is mainly controlled by the self-diffusivity of the base material. Thus, the composition is selected with the aim of maximizing the effective self-diffusivity of the base material at the sintering temperature.
4. The yield strength of the alloy with a single-phase microstructure having uniform grain size is controlled by the intrinsic strength and solid solution hardening only. Therefore, the composition is optimized to increase the solid solution strengthening of the final matrix.
5. To improve the pitting corrosion resistance of the alloy, the composition is also optimized to increase the equivalent chromium content (as defined in "Corrosion Resistance and Cost").
6. Finally, the composition is selected to minimize the cost per kilogram of the alloy.

Note that a higher effective self-diffusivity at a given temperature improves the sinterability of the powder compact by increasing the densification rate. An alloying element which increases the effective self-diffusivity of the powder compact might decrease the solid solution strengthening of the matrix and vice versa. However, improving the sinterability of the powder compact will also improve the yield strength through increasing the final density of the matrix. In addition, a powder compact that can densify faster will also have less grain growth during sintering.

Thus, based on the requirements drawn from the material system chart, a flexible model can be developed for designing a base powder composition that is capable of achieving the desired microstructure under the prescribed processing conditions.

Computational Methods

The design methodology involves single-criterion, multi-variable, and multi-objective optimization of the composition of a stainless steel alloy. It consists of an evolutionary (genetic) algorithm, which generates and evaluates candidate alloys based on feedback from (1) computational thermodynamics for microstructural stability and the effective self-diffusivity at the sintering temperature and (2) predictive analytical models

for the change in solid solution strengthening, pitting corrosion resistance and cost.

Computational Thermodynamics

Thermodynamic computations in the proposed design methodology are carried out using TC, a commercial software system based on the CALPHAD method [11]. In addition, determination of the effective kinetic/transport parameters for candidate alloys is also performed using the property diagram module of TC. For these purposes, the thermodynamic database for iron alloys, TCFE9, is coupled with the mobility database, MOBFE4, and results are accessed through Matlab using the TC-Matlab interface.

The phase fraction of candidate alloy systems at the required sintering temperature is calculated by TC based on minimization of the Gibbs free energy. This is used to select alloy candidates that satisfy the necessary criterion, as described in "Criterion for High-Temperature Microstructural Stability." In addition, calculation of the effective diffusion coefficient for candidate alloys helps to select those alloys according to their fitness to a defined objective function in the optimization.

Criterion for High-Temperature Microstructural Stability

As discussed in "Introduction" and "Material Systems for Stainless Steel Produced by MIM," the alloy is required to be a fully austenitic stainless steel. Thus, the high-temperature austenite stability of the candidate alloys is defined as a criteria or constraint in the design methodology. By using TC, the phase fractions of candidate alloys at high temperature can be calculated. This is achieved by single point equilibrium calculation for a given candidate alloy with known compositions of alloying elements, temperature, and pressure. Phase fractions of the given alloy can then be extracted from TC using the TC-Matlab interface. Those candidates with stable austenitic dispersions at high temperature are selected.

Computational Modeling of Effective Self-diffusivity

In this study, the green body is assumed to be made from spherical powders with uniform size and uniform spatial distribution. This results in sintering with uniform shrinkage without distortion, as well as a uniform distribution of pores and pore shapes. The grain size will be dependent on the initial particle size, the sintering time, and temperature and will be independent of alloy composition. It is therefore assumed that densification in the green body, with uniformly distributed powder particles, occurs mainly through lattice or self-diffusion of the base element. The higher the self-diffusivity, the greater the shrinkage rate at a given temperature. Thus, it is necessary to determine the effective self-diffusivity of the base element (Fe) in the stainless steel alloy.

The property diagram module of TC, together with the mobility database for iron, can be used to calculate the effective tracer-diffusivity, D_t, for a candidate alloy. This can be achieved by single point equilibrium calculation at a predefined temperature and pressure for a known composition of the solutes. The effective tracer diffusion coefficient of iron can then be extracted with the help of the TC-Matlab interface. The tracer diffusion coefficient is close to but not identical to the self-diffusion coefficient. However, the self-diffusion coefficient, D_s, is often related to the tracer diffusion coefficient by the following [12]:

$$D_s = D_t / f_c \tag{1}$$

where f_c is a correlation factor varying between 0.6 and 1.0 depending on the crystal structure and the diffusion mechanism. For diffusion dominated by the vacancy mechanism in a face centered cubic lattice, $f_c = 0.78$ [12]. Measurement of the tracer diffusion coefficient may sometimes be affected by grain boundary diffusion. Linnenbom et al. discussed the effect of grain boundary diffusion on the measurement of tracer diffusion coefficient in stainless steel alloys below a certain temperature [13]. For this study, estimation of the effective self-diffusivity using the tracer diffusion databases would thus be useful to account for grain boundary diffusion, if any, in the powder compact of the alloys in this study.

Predictive Models

This section presents details of the predictive models used to estimate the change in solid solution strengthening, pitting corrosion resistance, and cost for the given alloy composition during the computational design.

Change in Solid Solution Strength

For the alloy system in this study, work hardening can be ignored because the goal is only on yield strength. There will be no precipitation hardening in a single-phase fully austenitic material. The change in strength due to composition will therefore be dependent on solid solution strengthening and the sintered density only.

Solid solution strengthening occurs due to the interaction of stress fields between solute atoms and moving dislocations [14, 15]. The change in strength due to solid solution hardening in multi-component alloys depends on the solute content and misfit parameter that arises due to the change in size and rigidity. Analytical models for solid solution strengthening with few variations are reviewed by Weseman et al. [16]. However, the experimental determination of misfit parameters, especially for multi-component alloys with interstitial

solutes, is not always straight forward. With the aim of providing a practical formalism for integrated computational material engineering (ICME) in modeling solid solution strengthening, Walbruhl et al. suggested a generalized model for multi-component alloys based on an expansion similar to the Gibbs energy in thermodynamics using the compound energy formalism (CEF) [10]. Strengthening due to solid solution, σ_{sss}, at an isothermal temperature is given by the following:

$$\sigma_{sss} = \sum_{\alpha} f^{\alpha} \left[\sum_{i=1}^{N} \sum_{k>i}^{N} A^{\alpha}_{M_i M_k Va} \left(c'_{M_i} c''_{M_k} \right)^{q} c''_{Va} + \sum_{i=1}^{N} \sum_{j=1}^{n} A^{\alpha}_{M_i I_j Va} \left(c''_{Va} c''_{j} \right)^{r} c'_{M_i} \right] \tag{2}$$

where f represents the fraction of phase, α. The model considers the effect of substitutional as well as interstitial elements in strengthening or softening on the multi-component material separately. The first summation in the bracket represents strengthening due to addition of substitutional solutes, and it is performed over N substitutional elements. Thus, $A^{\alpha}_{M_i M_k}$ defines the strengthening parameter when a substitutional element, M_k, is added to M_i. The second summation represents contributions to strengthening due to addition of interstitial solutes, and hence, it is performed over n interstitial elements. Similarly, $A^{\alpha}_{M_i I_j}$ is a parameter defining strengthening when an interstitial, I_j, is added to substitutional element, M_i. The coefficients, q and r, are often chosen to be 2/3 as per the suggestion from Labusch et al. [15]. The concentration factors for each element are also defined as follows:

$$c'_i = \frac{c_i}{\sum_k^N c_k} \quad and \quad c''_j = \frac{c_j}{\sum_k^N c_k} g \tag{3}$$

where i and j denote the substitutional and interstitial elements, respectively. g is a constant that accounts for difference in interstitial sites depending on the crystal structure and takes a value of 1 for a fcc crystal structure.

Corrosion Resistance and Cost

The pitting corrosion resistance in a multi-component alloy is mainly dependent on the equivalent chromium composition. This is often represented by a factor called Pitting Resistance Equivalent, PRE, see Eq. (4), which represents the capacity of an alloy to resist pitting [17, 18].

$$\mathrm{PRE} = \%\mathrm{Cr} + 3\%\mathrm{Mo} + 16\%\mathrm{N} \tag{4}$$

A higher potential for corrosion is needed to initiate pitting in alloys with large PRE values than for alloys with lower values.

With regard to affordability of the alloy, the first criterion is the cost of the constituent elements. Processing cost is independent of the composition and hence can be ignored for comparison between different alloys processed by the same route. Thus, the cost is estimated using the price of the constituent metals per unit kilogram at the London Metal Exchange [19]. The relative cost of the alloy is calculated by considering the weight fraction of each metal element in the alloy.

Multi-variable Multi-objective Optimization Using GA

Genetic algorithms (GAs) are powerful tools to scan the enormous space of possible candidate alloys in order to optimize multi-variable, multi-objective problems with a predefined criterion/constraint. Inspired by the evolutionary selection process, following the survival of the fittest, a GA reproduces individuals so they evolve towards a defined objective solution. One of the advantages of GAs is that they work with populations instead of single solutions avoiding local solutions and arrive at global optima. In addition, the optimal result is not dependent on or determined by the initial solution. The evolution of individuals is controlled by probabilistic operators known as crossover and mutation rather than using predefined deterministic functions. GAs work effectively with binary representation of solution candidates consisting of strings of zeros and ones, often called chromosomes, requiring encoding/decoding procedures. Another important feature that makes GAs important for scanning compositional space in the design of alloys is that they make it easy to work with multi-objective optimizations through an objective function, which helps to prioritize or rank solutions relative to each other.

In this study, the so-called non-dominated sorting genetic algorithm (NSGA-II) [20] is adopted to carry out the multi-objective optimization task. Non-dominated sorting means that when two feasible individuals are compared, the Pareto-optimal one is selected. Thus, the NSGA-II provides a set of non-dominated optimal solutions. Note that, while working with a multi-objective optimization problem, it is often difficult to achieve all the aspirations with a single best solution; rather, a set of mutually non-dominant solutions represents optimality. This is known as a Pareto set. If any member of the Pareto set is better than the other in terms of one objective, it will be inferior in terms of another objective [21].

Four objectives are considered: maximizing the effective self-diffusivity, maximizing solid solution strengthening, maximizing pitting corrosion resistance, and minimizing cost per kilogram. The optimization algorithm is implemented using Matlab™ with a flowchart shown in Fig. 2a. Individual alloy candidates are considered as chromosomes having genes representing the percentage by weight of each element in the alloy, see Fig. 2b. A set of these individuals with different elemental compositions (genes) is called a population (pop). The population undergoes reproduction

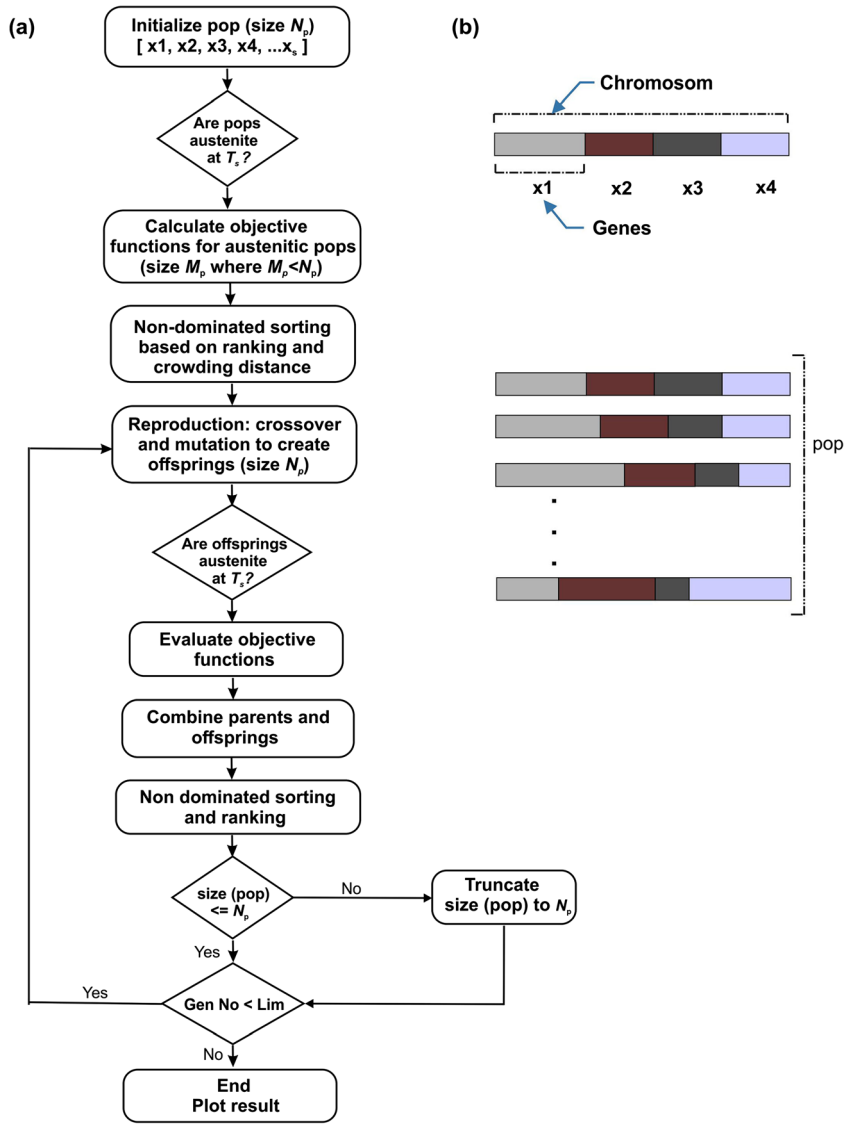

Fig. 2 **a** Flowchart of the genetic algorithm. **b** Example of Individual chromosome with four genes representing four elements in the alloy

enabling the individual candidates to evolve, through varying the values of the genes, according to their fitness to the objective function.

The NSGA-II employed in this study involves the following steps, see Fig. 2a:

1. An initial set of N_p individuals (population) consisting of the weight percentage of s substitutional and i interstitial elements are generated randomly within a predefined range (bound) for each element.
2. The phase fractions are calculated using ThermoCalc for each of the individual candidates at the sintering temperature. From the entire population, M_p candidates ($M_p < N_p$) with fully austenitic phase are selected. If the number of austenitic candidates, M_p, is less than 25, the algorithm will generate a new set of individuals once again so that there are enough individuals for reproduction. This step tests the individual candidates for the criterion discussed in "Criterion for High-Temperature Microstructural Stability."
3. For each of the M_p candidates, the effective self-diffusion coefficient (D_s), change in strength due to solid solution hardening ($\Delta\sigma_{sss}$), pitting resistance equivalent (PRE), and cost of the alloy are calculated using ThermoCalc and the predictive models discussed in "Computational Modeling of Effective Self-diffusivity" and "Predictive Models," respectively.
4. Non-dominated sorting of the M_p candidate is then performed using ranking and crowding distance [20].
5. Reproduction by crossover and mutation is then performed on the set of individuals (population) obtained from step 4 to produce offspring (children).
6. The microstructural stability of the offspring population is tested. Those that are austenite at the sintering temperature

are combined with the parents and sorted according to their ranking and crowding distance.

7. To diversify the pool of candidates after every iteration, a new set of randomly generated individuals, about 5% of the population after reproduction, are added. This enhances the search performance by diversifying the solution space and helps to avoid convergence to local optima.
8. The reproduction continues until the number of generations (Gen no) reaches a predefined limit (Lim).

Application of the Design Method

In this section, an example of the computational method proposed in this study is presented. Design inputs are presented first, including the composition and solid solution strengthening model parameters, followed by the results and discussion.

Compositional Bounds

The concentration range/bound of each element considered is shown in Table 1, with the composition of austenitic alloy 316L shown for comparison. The concentration of interstitial elements is fixed whereas the substitutional elements are allowed to vary between the minimum (Min) and maximum (Max) limit. Two cases were considered depending on the presence of copper (Cu) and the interstitial concentration. Here, the total composition of the alloying elements is kept below 50%.

Model Parameters for Solid Solution Strengthening

The general model discussed in "Change in Solid Solution Strength" is based on the explicit description of the strengthening parameters for substitutional, $A^{\alpha}_{M_iM_k}$, as well as interstitial, $A^{\alpha}_{M_iI_j}$, elements in the alloy system. This requires the determination of the model parameters, including those for interstitial elements.

Table 1 Composition bound/range of alloying elements (wt%)

Element	316L	Case A		Case B	
		Min	Max	Min	Max
Fe	Bal	Bal	Bal	Bal	Bal
Cr	17	11	25	11	24
Ni	12	8	15	8	14
Mo	2.5	1	4	1	4
Mn	1	0	3	0	3
Cu	–	–	–	0	3
C (fixed)	0.03	–	0.03	–	0.06
Si (fixed)	0.75	–	0.75	–	0.95
N (fixed)	0.10	–	0.10	–	0.12
P (fixed)	0.04	–	0.04	–	0.04
S (fixed)	0.03	–	0.03	–	0.03

Ohkubo et al. [22] and Kako et al. [23] reported a detailed study on the effect of alloying elements on the strength of austenitic stainless steels. They presented the change in 0.2% proof strength (PS), $\Delta\sigma_{0.2}$, as a function of change in concentration of nine alloying elements. Parameters for modeling the solution strengthening were determined by adapting and fitting the model in Eq. (2), to the change in 0.2% PS due to the variation in a given alloying element, *elem*, as follows:

$$\Delta\sigma_{0.2}^{elem} = \Delta\sigma_{sss}^{elem} \tag{5}$$

Equation (5) indicates that the observed changes in yield strength associated with changes in composition of a given alloying element is due to solution hardening, assuming that all alloys are sintered to the same density. For example, the observed variation in 0.2% PS of the austenitic steel due to change in composition of chromium, Δc_{Cr} from the base composition, is related to the solution hardening model to determine the parameter, A_{FeCr}, as follows:

$$\Delta\sigma_{0.2}^{\Delta\mathrm{Cr}} = A_{FeCr}\left(c'_{\mathrm{Fe}}\Delta c''_{\mathrm{Cr}}\right)^{q} c''_{\mathrm{Va}} \tag{6}$$

where c'_{Fe} and c''_{Va} are calculated using the base composition of the austenitic steel. Unlike the classical models for solution hardening, the model in Eq. (2) does not require explicit assessment of misfit parameters. The model considered in this study will help to convolute or bundle the effect of misfit as well as other factors (e.g., possible change in average grain size due to addition of an element) into a single parameter to simplify the modeling of solution hardening.

All the parameters determined for the alloying elements considered in this study are shown in Eq. (7). Note that the combination of elements that have a secondary effect on strengthening, for example, contributions from a combination of nickel (Ni) and molybdenum (Mo), A_{NiMo}, on the overall strength of the austenitic alloy is negligible as the concentration of those elements is small. Thus, the strengthening parameters for these kinds of combinations are assumed to be one. In other words, strengthening in the austenitic steel is primarily determined by a combination of the solute with the base element (Fe) and hence values in the first row of Eq. (7) need to be determined accurately.

The strengthening parameters for elements like Ni, Mn, and Cu are found to be less than zero, indicative of a softening effect. This is also discussed in detail by Ohkubo et al. [22] and Dulieu et al. [24] and explained by the change in stacking fault energy. Further description and verification with regard

to the effect of Cr and Ni on the stacking fault energy and hence strength of austenitic steels are also reported by Vitos et al. [25] after performing detailed atomistic simulations with the help of density functional theory.

$$\begin{bmatrix} A_{FeCr} & A_{FeNi} & A_{FeMo} & A_{FeMn} & A_{FeCu} \\ & A_{CrNi} & A_{CrMo} & A_{CrMn} & A_{CrCu} \\ & & A_{NiMo} & A_{NiMn} & A_{NiCu} \\ & & & A_{MoMn} & A_{MoCu} \\ & & & & A_{MnCu} \end{bmatrix} = \begin{bmatrix} 338.1 & -330.5 & 317.2 & -179.2 & -277.4 \\ & 107.3 & 1.0 & 1.0 & 1.0 \\ & & 1.0 & 1.0 & 1.0 \\ & & & 1.0 & 1.0 \\ & & & & 1.0 \end{bmatrix} \quad (7)$$

Among the interstitial elements listed in Table 1, carbon (C), nitrogen (N), and silicon (Si) cause significant hardening in austenitic alloys, although their concentration is very small [22, 23]. Thus, the parameters defining strengthening when carbon, nitrogen, and silicon are added to the alloy system are determined to be $A_{FeC} = 2340, A_{FeN} = 3250, and\ A_{FeSi} = 4100$. The strengthening parameters for the remaining interstitial elements, i.e., phosphorous (P) and sulfur (S), have almost no solution hardening effect as shown by Kako et al. [23] and are assumed to be one.

Results and Discussion

Results from a design exercise using the proposed method are presented in this section. The Pareto-frontier for the first and second objectives, i.e., change in solid solution strengthening and the effective self-diffusivity, is calculated. Improvements in sintering behavior and yield strength for the resulting optimal solutions are also discussed, particularly in comparison to 316L grade austenitic stainless steel.

Effect of Alloying Elements on the Effective Self-diffusivity

The effective self-diffusivity of iron (Fe) in stainless steel is affected by the composition of solute elements. Figure 3 shows the variation in the effective self-diffusivity of iron with the composition of the main alloying elements in stainless steel, i.e., Cr, Ni, Mo, Mn, and Cu at 1600 K, as calculated using the property diagram module of TC. The effective self-diffusivity of iron in the alloy is calculated by varying the percentage by weight of one of the solutes between the minimum and maximum value shown in Table 1, while keeping the composition of the other elements constant (at their mid value). An isothermal temperature of 1600 K is chosen because it is the optimal sintering temperature for austenitic stainless steels [26].

Within the respective composition bounds, chromium, manganese, and copper are found to increase the effective self-diffusivity of iron in stainless steel alloys, whereas the addition of molybdenum has the opposite effect. Nickel is observed to have a very small effect on the self-diffusivity of iron within the compositional bound considered in this study. The increase in diffusivity due to the addition of chromium in stainless steel could be attributed to the slightly bigger size of the chromium atom inducing mismatch strain in the face centered cubic lattice and hence reducing the activation energy for the diffusion of iron atoms. On the other hand, manganese and copper are known to increase the stacking fault energy of the fcc lattice, which enhances the diffusion of vacancies in the crystal structure [22].

Optimal Solutions

It was observed that improvement stagnates for all concentrations of all alloying elements after 300 generations, as shown in Fig. 4. Hence, a maximum of 300 generations was chosen as the stopping criterion, which is equivalent to a computational time of a few days using personal computers.

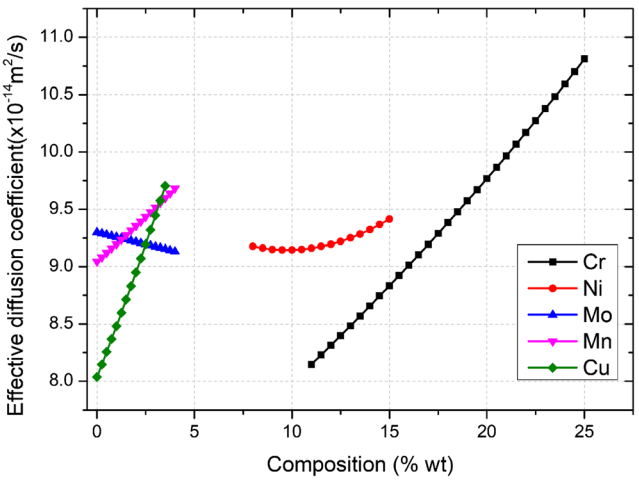

Fig. 3 Effect of substitutional alloying elements on the effective self-diffusivity of iron in stainless steel

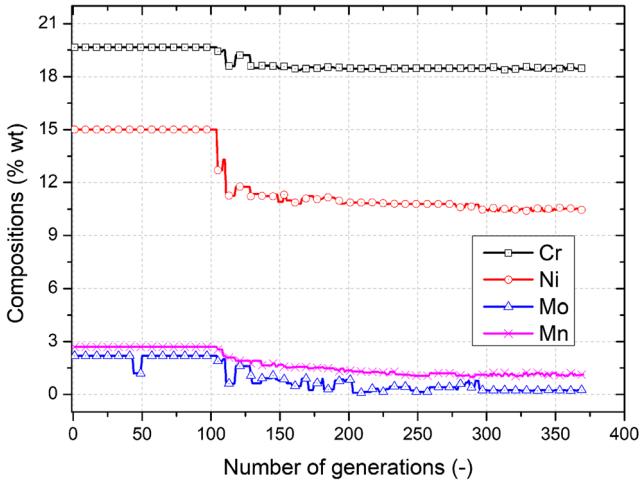

Fig. 4 Composition of the substitutional alloying elements as a function of number of generations (for case A compositional bound)

The population size was set to $N_p = 500$. Genetic operations were performed using the encoded binary crossover and a uniform mutation operator. When generating the offspring population, the probability for an individual to serve as a parent, the crossover probability, was $P_c = 0.7$. The probability for an individual to be mutated was set to $P_m = 0.12$. The mutation operation selected new random values for each gene; these values were uniformly drawn between the genes respective lower and upper bounds.

Figure 5 shows the Pareto set, after the optimal solutions are achieved, for the two compositional bounds discussed in "Compositional Bounds." Solutions in the Pareto set (Pareto-frontier) are plotted considering the first and second objectives in the optimization, i.e., change in solid solution strengthening versus the effective self-diffusivity. Note that each point in the Pareto set represents a unique alloy with its own composition that is an optimal trade-off

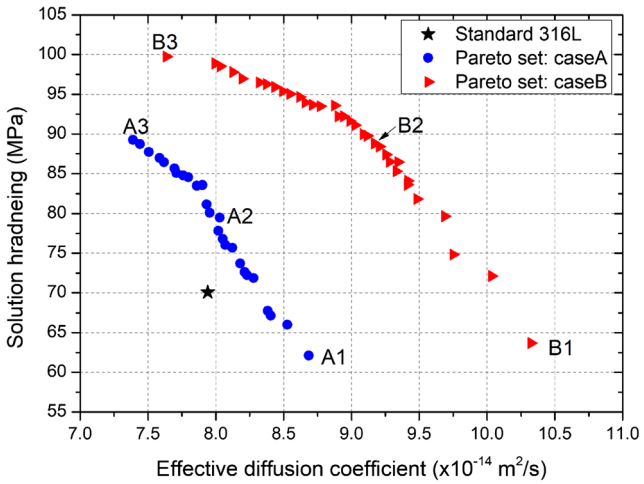

Fig. 5 Pareto frontier for change in solid solution strength versus effective self-diffusivity for two cases of compositional ranges

to the four objective functions considered in the study. For the sake of comparison, the standard 316L alloy is also shown in the Fig. 5. This demonstrates that the composition of austenitic stainless steels can be altered to maximize the effective self-diffusivity and/or the change in solid solution hardening. Note that all the points in both Pareto-frontiers shown in Fig. 5 are optimal in the sense that it is possible to improve one objective only by making the other worse. Thus, the choice of the "best" alloy from the Pareto set depends on the users' priority.

For example, the Pareto sets obtained using case B compositional bounds, see Table 1 and Fig. 5, are shown to have higher self-diffusivity of iron as well as solution hardening compared to case A. Generally, comparison of Pareto optimal solutions in case A and B compositional bounds show that by adding copper (Cu), it is possible to maximize the effective self-diffusivity of iron and achieve better sinterability of the alloy. Furthermore, addition of a small amount of carbon (C) and silicon (Si) is also found to push the Pareto-frontier up resulting in higher solution hardening. Note that the final yield strength of the alloy depends not only on the solution hardening but also on the final density after sintering. Comparison of the change in yield strength after sintering for equal durations of the three optimal alloys from each of the two Pareto sets, shown in Fig. 5 as A1/B1, A2/B2, and A3/B3, is discussed in "Properties of Optimal Alloys."

Properties of Optimal Alloys

Improvement in the sintering behavior of the optimal alloys is demonstrated by comparing their densification behavior with that of a commercially available austenitic stainless steel (316L). For this purpose, a solution from the Pareto set with the maximum effective self-diffusivity is chosen. Solid-state sintering of a powder compact during MIM is assumed to be governed by lattice diffusion that can be modeled by considering the modified version of the Nabarro-Herring creep equation [12]. Thus, the linear shrinkage or strain rate, $\dot{\varepsilon}_L$, during sintering at isothermal temperature, T, is given by the following:

$$\dot{\varepsilon}_L = \frac{\dot{\rho}}{3\rho} = \frac{40}{3}\left(\frac{D_s\Omega}{G^2kT}\right)D_F \tag{8}$$

where ρ represents the relative density and $\dot{\rho} = d\rho/dt$, D_s is the lattice or self-diffusion coefficient, Ω is the atomic volume, G is the particle size, k is the Boltzmann constant, and D_F is the driving stress for sintering. Since there is no external application of load on the sample during sintering in the MIM process, the driving force for sintering is the intrinsic sintering stress, σ_s, and hence $D_F = \sigma_s$. The intrinsic sintering stress

depends on the specific surface energy, γ_s, amount of porosity, θ, and curvature of pores in the powder compact, and it can be given by the following [27]:

$$\sigma_s = \frac{3\gamma_s}{2G}(1-\theta)^2 \tag{9}$$

By combining Eqs. (8) and (9), the linear shrinkage rate of the powder compact is given by the following:

$$\dot{\varepsilon}_L = 20\left(\frac{D_s\Omega\gamma_s}{G^3kT}\right)(1-\theta)^2 \tag{10}$$

Considering conservation of mass, the volumetric shrinkage/strain rate, $\dot{\varepsilon}_V$, of a powder compact during sintering can also be expressed in terms of porosity, θ, where $\theta = 1-\rho$, as follows [27]:

$$\dot{\varepsilon}_V = 3\dot{\varepsilon}_L = \frac{\dot{\theta}}{1-\theta} \tag{11}$$

Coarsening of particles during sintering is considered using an inverse square-root function usually used for metallic powders involving a grain growth coefficient k' and an initial particle size, G_0, as follows [28]:

$$G = \frac{k'G_0}{(1-\rho)^{1/2}} \tag{12}$$

Jamaludin et al. [26] reported the optimal sintering conditions for an austenitic stainless steel after performing optimizations using the so-called design of experiment (DOE) method. They suggested an optimal sintering temperature close to 1600 K for 316L, with an initial particle size of 7 μm [26]. These conditions are thus used to compare densification between 316L and the optimal alloys obtained in this study. Using the effective self-diffusion coefficients of the optimal alloys obtained from the optimization procedure, densification in the alloy's powder compact is modeled using Eqs. (10)–(12). Table 2 shows the parameters used during modeling the sintering behavior of 316L and the new optimal alloys obtained using the two cases of compositions bounds discussed in "Compositional bounds."

Table 2 Parameters used in the sintering model

Sintering temperature, T (K)	1600
Initial particle size, G_o (μm)	7.00
Initial porosity, θ_0 (–)	0.20
Atomic volume, Ω (m^3)	1.18×10^{-29}
Specific surface energy, γ_s (J/m^2)	2.60
Boltzmann constant, k (J/K)	1.38×10^{-23}
Grain growth coefficient, k' (–)	0.50

Figure 6 shows a comparison of the relative density as a function of sintering time between 316L and the two optimal alloys obtained using the two compositional ranges (cases A and B in Table 1). The dwell time for 316L (close to 250 min) is found to be consistent with the optimal time reported by Jamaludin et al. [26]. Comparison of dwell time between 316L and the optimal alloy for case A compositional bound shows a modest improvement. However, the optimal alloy from case B compositional bound is observed to have a 25% reduction in the dwell time compared to 316L.

Variation of strength of metals with relative density is often expressed with the help of an empirical exponent, b, to the relative density [29]. If solution hardening is the only strengthening mechanism, the effective change in yield strength of a metallic alloy, $\Delta\sigma_y^{alloy}$, after sintering can be given by the following:

$$\Delta\sigma_y^{alloy} = \sigma_{sss}\cdot\rho^b \tag{13}$$

Combining Eqs. (10) and (11) and solving for the evolution of relative density as a function time, t, during sintering gives the following:

$$\rho = \rho_0\exp\left(40\frac{\Omega D_s\sigma_s}{G^2kT}t\right) \tag{14}$$

where ρ_0 is the initial relative density of the powder compact. By combining Eqs. (13) and (14), the effective change in yield strength of the alloy as a function of relative density is given by the following:

$$\Delta\sigma_y^{alloy} = \sigma_{sss}\left[\rho_0\exp\left(40\frac{\Omega D_s\sigma_s}{G^2kT}t\right)\right]^b \tag{15}$$

Assuming a linear variation of strength with relative density, i.e., $b = 1$, the effective change in yield strength of the

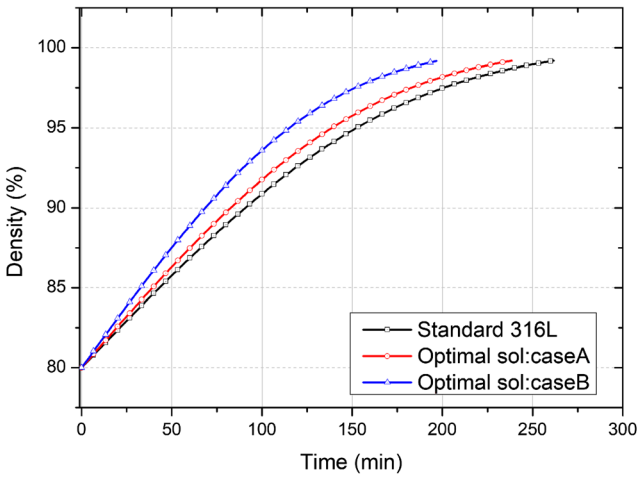

Fig. 6 Comparison of the densification behavior of the optimal alloys obtained from cases A and B with an existing austenitic stainless steel, 316L

alloy powder compact with an initial relative density of, ρ_0, sintered at an isothermal temperature of, T, for a time, t, is given by the following:

$$\Delta\sigma_y^{alloy} = \sigma_{sss}\rho_0 \exp\left(40\frac{\Omega D_s \sigma_s}{G^2 kT}t\right) \quad (16)$$

The change in yield strength of the optimal alloys after sintering for 190 min can thus be calculated using Eq. (16). Figure 7 summarizes the relationship between cost per kilogram of the optimal alloys with enhancement of pitting corrosion resistance (PRE) and yield strength. A surface fitted to the 3D data points show that increasing the yield strength can be achieved without a significant cost increment whereas an increase in corrosion resistance incurs additional cost.

The change in yield strength after sintering for 190 min for three representative optimal alloys from each of the Pareto sets (A1/B1, A2/B2, and A3/B3) from Fig. 5 is shown in Table 3. Comparison of the corresponding points from the two cases shows that all alloys in the case B (B1, B2, B3) show a larger change in yield strength than case A. The improvement in yield strength is achieved not only because of higher solution hardening but also via improved densification. With regard to corrosion resistance and cost, all three solutions (from each of the Pareto sets) are comparable to that of 316L, see Table 3. Therefore, improved sinterability and a larger change in yield strength can be achieved without significantly higher cost. However, as shown in Fig. 7, improvements in corrosion resistance require additional cost. By performing this kind of comparison between the different Pareto optimal solutions, it is possible to make an informed decision for an improved alloy.

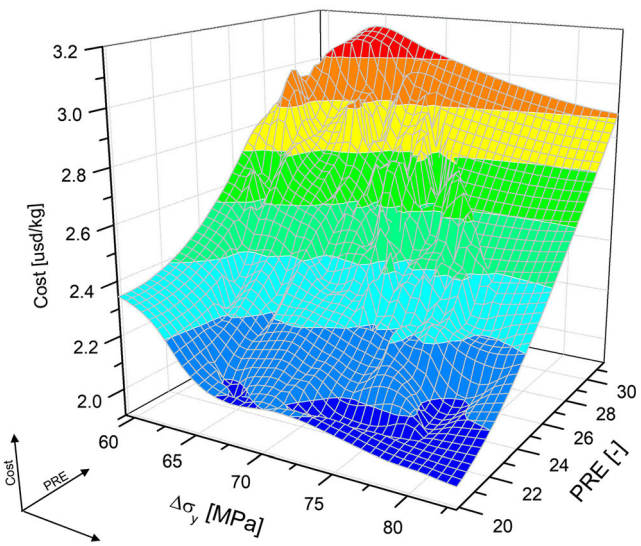

Fig. 7 Plot of cost of the alloy as a function of change in yield strength and corrosion resistance (PRE)

Table 3 Comparison of three optimal alloys from two cases of compositional bounds after sintering for 190 min

	316L	Pareto set: case A			Pareto set: case B		
		A1	A2	A3	B1	B2	B3
ρ_f (%)	95.76	97.55	96.63	96.13	98.96	97.82	96.44
$\Delta\sigma_y$ (MPa)	66.58	60.60	73.85	85.81	63.94	88.73	96.20
PRE (–)	24.5	24.82	23.32	24.20	25.57	27.60	25.45
Cost (USD/kg)	2.51	2.53	2.24	2.18	2.07	2.30	2.02

During mass production of components from multi-component alloys using MIM, optimizing the powder mix for sinterability is important for shortening the sintering cycle and hence reducing cost. In this respect, the present study demonstrates possibilities for new austenitic stainless steel alloys which have improved sinterability, yield strength, and corrosion resistance. The computational design method proposed in this study can be used for fast realization of the properties of austenitic stainless steels produced by MIM. The design methodology is flexible in that it can incorporate additional properties such as toughness and ductility. The methodology suggested in this study can also be extended further by coupling additional submodels to calculate the effective diffusion coefficient to account for different particle sizes or multi-phase alloys.

Conclusion

A new computational methodology for designing austenitic stainless steel alloys with improved sintering behavior is developed. The design method follows the material systems approach that integrates processing, structure, and property (PSP) relations during metal injection molding (MIM). The material system chart for austenitic stainless steels shows that preparation of the powder mix and sintering is the two critical steps determining the structure and hence properties during MIM. Therefore, the design methodology is developed to simultaneously optimize four independent objectives: sinterability, yield strength, pitting corrosion resistance, and cost. Focus is given to improved manufacturability during MIM, particularly sinterability of the powder compact by maximizing the effective self-diffusivity of the alloy at high temperature.

The computational methodology involves a multi-objective optimization, using a genetic algorithm (GA) and integrating computational thermodynamics- and physics-based predictive models. Alloy candidates, with predefined compositional bounds for each of the constituent elements, are generated randomly using the capabilities of a GA. The equilibrium state of a given alloy candidate at given sintering temperature is determined using computational thermodynamics to identify and

select those candidates with a fully austenitic composition. Equilibrium state calculations are performed based on the CALPHAD method using the ThermoCalc (TC) software. TC is also coupled with a mobility database to determine the effective self-diffusivity of the candidate alloy, which determines the sinterability (densification behavior of the powder compact) at high temperature. The GA, based on non-dominated sorting of solutions, is then used to improve the optimal alloy composition based on feedback from the computational thermodynamics and the predictive models.

The design methodology is shown to provide a non-dominated set of optimal alloys (Pareto set). To demonstrate the capability of the design approach, properties of the optimal alloys for two cases of compositional bounds are compared to a commercially available austenitic stainless steel, 316L. The densification rate (measured in terms of dwell time) of the optimal alloys can be reduced by 25% (64 min) compared to 316L. It is also shown that an increase in yield strength can be achieved without a significant cost penalty whereas an increase in corrosion resistance always incurs additional cost. The methodology can be extended by coupling additional submodels so that additional properties or microstructural complexity can be incorporated in the design space.

References

1. Olson GB (1997) Computational design of hierarchically structured materials. Science (80-.). 277:1237–1242
2. Matouš K, Geers MGD, Kouznetsova VG, Gillman A (2017) A review of predictive nonlinear theories for multiscale modeling of heterogeneous materials. J Comput Phys 330:192–220
3. Tancret F, Bhadeshia HKDH, MacKay DJC (2003) Design of a creep resistant nickel base superalloy for power plant applications: part 1—mechanical properties modelling. Mater Sci Technol 19:283–290
4. Tancret F, Bhadeshia HKDH (2003) Design of a creep resistant nickel base superalloy for power plant applications: part 2—phase diagram and segregation simulation. Mater Sci Technol 19:291–295
5. Tancret F (2013) Computational thermodynamics, Gaussian processes and genetic algorithms: combined tools to design new alloys. Model Simul Mater Sci Eng 21:0–9
6. Jha R, Pettersson F, Dulikravich GS, Saxen H, Chakraborti N (2015) Evolutionary design of nickel-based superalloys using data-driven genetic algorithms and related strategies. Mater Manuf Process 30:488–510
7. Mahfouf M, Jamei M, Linkens DA (2005) Optimal design of alloy steels using multiobjective genetic algorithms. Mater Manuf Process 20:553–567
8. Menou E, Ramstein G, Bertrand E, Tancret F (2016) Multi-objective constrained design of nickel-base superalloys using data mining- and thermodynamics-driven genetic algorithms. Model Simul Mater Sci Eng 24:055001
9. Li S, Kattner UR, Campbell CE (2017) A computational framework for material design. Integr Mater Manuf Innov 6:229–248
10. Walbrühl M, Linder D, Ågren J, Borgenstam A (2017) Modelling of solid solution strengthening in multicomponent alloys. Mater Sci Eng A 700:301–311. https://doi.org/10.1016/j.msea.2017.06.001
11. Perrut M (2015) Thermodynamic modeling by the CALPHAD method and its applications to innovative materials. J AerospaceLab 1–11
12. Rahaman MN (2008) Sintering of ceramics, Taylor and Francis Group, Boca Raton, FL
13. Linnenbom V, Tetenbaum M, Cheek C (1955) Tracer diffusion of Iron in stainless steel. J Appl Phys 26:932–936
14. Fleischer RL (1961) Solution hardening. Acta Metall 9:996–1000
15. Labusch R (1970) A statistical theory of solid solution. Phys Status Solidi B 41:659–669
16. Wesemann I, Hoffmann A, Mrotzek T, Martin U (2010) Investigation of solid solution hardening in molybdenum alloys. Int J Refract Met Hard Mater 28:709–715
17. McGuire MF (2008) Stainless steels for design engineers, ASM International, https://www.asminternational.org/search/-/journal_content/56/10192/05231G/PUBLICATION (accessed March 22, 2018)
18. Bhandari J, Khan F, Abbassi R, Garaniya V, Ojeda R (2015) Modelling of pitting corrosion in marine and offshore steel structures—a technical review. J Loss Prev Process Ind 37:39–62
19. London metal exchange: home, (n.d.). https://www.lme.com/ (accessed March 22, 2018)
20. Deb K (2011) Multi-objective optimization using evolutionary algorithms: an introduction, http://www.iitk.ac.in/kangal/deb.htm (accessed May 1, 2018)
21. Shukla PK, Deb K (2006) On finding multiple Pareto-optimal solutions using classical and evolutionary generating methods
22. Ohkubo N, Miyakusu K, Uematsu Y, Kimura H (1994) Effect of alloying elements on the mechanical properties of the stable austenitic stainless steel. ISIJ Int 34:764–772
23. Kako K, Kawakami E, Ohta J, Mayuzumi M (2002) Effects of various alloying elements on tensile properties of high-purity Fe-18Cr-(14-16)Ni alloys at room temperature. Mater Trans 43:155–162
24. Rönnquist A, Dulieu D (1964) On the determination of stacking fault energies in austenitic stainless steel by the method of extended node measurements. Br J Appl Phys 15:1569–1571
25. Vitos L, Nilsson JO, Johansson B (2006) Alloying effects on the stacking fault energy in austenitic stainless steels from first-principles theory. Acta Mater 54:3821–3826
26. Jamaludin KR, Muhamad N, Rahman MNA, Amin SYM, Ahmad S, Ibrahim MHI (2016) Sintering parameter optimisation of the SS316L metal injection molding (MIM) compacts for final density using Taguchi method, 3rd South East Asian Tech. Univ Consort Symp:258–262
27. Olevsky EA (1998) Theory of sintering: from discrete to continuum. Mater Sci Eng R-Reports 23:41–100
28. German RM (2010) Coarsening in sintering: grain shape distribution, grain size distribution, and grain growth kinetics in solid-pore systems. Crit Rev Solid State Mater Sci 35:263–305
29. Chen X, Wu S, Zhou J (2013) Influence of porosity on compressive and tensile strength of cement mortar. Constr Build Mater 40:869–874